Nanoscale

PAPER

View Article Online
View Journal | View Issue

Published on 06 November 2017. Downloaded by NANJING UNIVERSITY on 03/12/2017 14:30:00.

Check for updates

Cite this: *Nanoscale*, 2017, **9**, 18546

Coupled relaxation channels of excitons in monolayer $MoSe_2$†

Bo Liu,[a] Yuze Meng,[b] Xuezhong Ruan,*[a] Fengqiu Wang,*[a] Wengqin Liu,[c] Fengqi Song,[b] Xuefeng Wang,[a] Jing Wu,[c] Liang He,[a] Rong Zhang[a] and Yongbing Xu*[a,c]

Received 16th July 2017,
Accepted 4th November 2017

DOI: 10.1039/c7nr05174c

rsc.li/nanoscale

Using ultrafast degenerate pump–probe spectroscopy, we have investigated the ultrafast exciton dynamics of monolayer $MoSe_2$ at different pump fluences. The exciton–exciton annihilation, typically occurring tens of picoseconds after pump excitation, has been found to have a substantial correlation with the initial relaxation process dominated by the defect trapping of excitons. A new exciton–exciton annihilation model has been proposed by introducing a coupling term that accounts for the initial relaxation contribution. This coupling term can be tuned by varying the pump excitation intensity and at a high intensity it vanishes due to the full occupation of the defect states. At the same time, the final electron–hole recombination is found to be affected by the heat accumulation effect originating from the high intensity pump pulses.

1 Introduction

Photo-generated excitons in monolayer transition metal dichalcogenides (TMDCs) have been widely investigated in recent years due to their excellent optical properties. Emerging TMDC materials, such as MoS_2, $MoSe_2$, WS_2 and WSe_2, have sizable bandgaps that change from an indirect bandgap to a direct bandgap when reduced to a monolayer. This electronic bandgap change leads to an extreme enhancement of photoluminescence (PL),[1] which makes these atomically thin materials well suited to a variety of optoelectronic applications, such as LEDs,[2] photodetectors,[3] and photovoltaics.[4] In addition, due to the high exciton binding energy[5–8] (on the order of hundreds of meV), these materials have good stability even at room temperature for the application of optoelectronic devices.[9–11] To apply TMDCs in future optoelectronic devices, it is very important to understand the dynamic behavior of excitons or carriers excited by light. The temporal characteristics of excitons or carriers will determine the performance of the LEDs or photodetectors. Recently, the exciton dynamics in monolayer TMDCs has been investigated *via* both time-resolved PL and transient pump–probe spectroscopy techniques. According to the time-resolved PL measurements[12–14] as well as the theoretical calculations,[15,16] the average radiative lifetime of excitons in TMDCs varies from a few picoseconds at a low temperature to hundreds of picoseconds or even nanoseconds at room temperature. In addition to the radiative recombination, various exciton scattering mechanisms are revealed through the pump–probe spectroscopy. Exciton–exciton annihilation, an efficient exciton relaxation mechanism occurring within a few tens of ps, has been observed in atomically thin MoS_2 [17] and $MoSe_2$.[18] Several groups attribute the initial relaxation process within a few ps in single layer MoS_2 to defect state trapping,[19,20] but Nie *et al.*[21] interpret the same span as the carrier cooling. Although different kinds of scattering mechanisms have been proposed, the microscopy mechanisms governing the relaxation process of excitons (or carriers) in TMDCs are still not fully clear. In these previous studies, each of the relaxation stages was found to be dominated by a specific relaxation mechanism. It is important to explore whether any of these mechanisms are coupled or not, as these mechanisms might occur in a wide time scale leading to their possible overlaps. Addressing such an aspect will be critical in understanding the relatively complex photo-physics and manipulating the exciton lifetime in TMDCs.

In this article, by employing degenerate pump–probe spectroscopy, we find clear evidence of the correlation between two exciton relaxation channels, where the initial fast decay component facilitates the subsequent exciton–exciton annihilation process in monolayer $MoSe_2$. A coupling term is introduced to

[a]*Jiangsu Provincial Key Laboratory of Advanced Photonic and Electronic Materials, Collaborative Innovation Center of Advanced Microstructures, School of Electronic Science and Engineering, Nanjing University, Nanjing 210093, People's Republic of China. E-mail: xzruan@nju.edu.cn, fwang@nju.edu.cn, ybxy@nju.edu.cn*
[b]*Department of Physics, Nanjing University, Nanjing 210093, People's Republic of China*
[c]*York-Nanjing International Joint Center in Spintronics, Departments of Electronics and Physics, The University of York, York YO10 5DD, UK*
†Electronic supplementary information (ESI) available. See DOI: 10.1039/C7NR05174C

This journal is © The Royal Society of Chemistry 2017

Published on 06 November 2017. Downloaded by NANJING UNIVERSITY on 03/12/2017 14:30:00.

account for the influence of the initial defect trapping process on the following exciton–exciton annihilation. The contribution of this coupling term is found to decrease with the increase of the pump fluence until the saturation of the defect states at high fluences. The final stage of relaxation, which lasts hundreds of picoseconds, is attributed to electron hole recombination as no dependence of the relaxation time on pump injected exciton density is found at a low pump fluence.

2 Experimental section

We performed the degenerate pump–probe spectroscopy of which the experimental configuration is shown in Fig. 1(a), with the pump and probe wavelengths being the same. To avoid the pump beam scattering into the detectors, the probe beam is at normal incidence while the pump beam is around 40 degrees away from the normal direction of the sample plane. This configuration allows us to spatially separate the reflected pump and probe beams. The probe beam is focused on the sample using an aspheric lens with a spot size of about 20 μm in diameter. Whereas the pump beam is focused by using another lens and its spot size is about 38 μm. Fig. 1(b) shows the diagram of the conduction and valence bands of monolayer $MoSe_2$ at a K valley. The red arrows represent the degenerate pump–probe excitation at A-exciton resonance. The $MoSe_2$ samples are grown by the chemical vapor deposition (CVD) method with a size larger than 100 × 100 μm and all the measurements are performed at room temperature. In this measurement, the polarization of pump and probe beams is orthogonal to each other to further avoid the scattering of pump beams. Under the excitation of a 532 nm laser, strong photoluminescence with a central wavelength of 800 nm, a fingerprint of the monolayer $MoSe_2$, is observed, as shown in Fig. 1(d) (black solid line). Fig. 1(c) presents the Raman spectrum of monolayer $MoSe_2$ and the peak at the wave vector of 239.72 cm^{-1} corresponds to the out-of-plane phonon mode A_{1g}. The similar Raman spectral behavior of monolayer $MoSe_2$ is also reported in many other studies.[22–24] The in-plane mode E_{2g} is not clear, which may be due to the defect impact. The optical image in the inset of Fig. 1(c) shows a typical monolayer $MoSe_2$ flake used in our measurement.

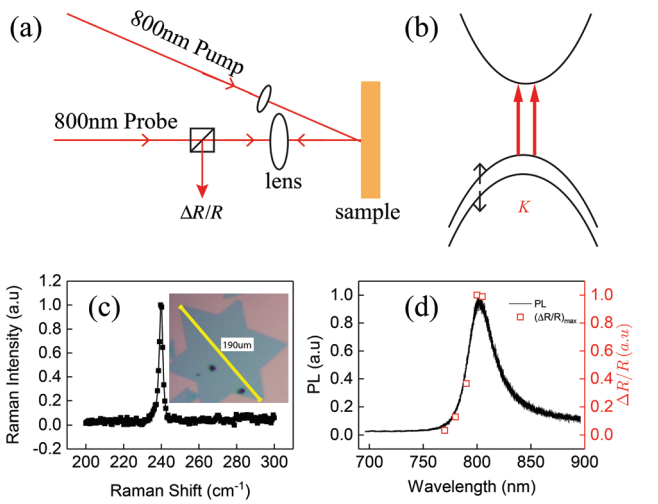

Fig. 1 (a) Diagram of the experimental geometry and optical characteristic. Both wavelengths of the pump and the probe are 800 nm and the incident angle of the pump beam is around 40°. The probe beam is normally incident. (b) Schematic diagram of the conduction and valence bands at the K valley of monolayer $MoSe_2$. The red arrows represent degenerate pump–probe excitation at A-exciton energy. (c) Raman spectroscopy and the inset is the optical microscopy image of monolayer $MoSe_2$. The sample size is about 190 μm illustrated by the scale bar. (d) Photoluminescence (PL) spectra and peak differential reflectivity signals as a function of the pump–probe energy (red squares) of monolayer $MoSe_2$.

3 Results and discussion

Fig. 2(a) shows the transient reflectivity of monolayer $MoSe_2$ measured at different values of the pump fluence. We perform these measurements under the wavelength of 800 nm. For clarity, we only present the data below the pump fluence of 1.16 μJ cm^{-2}. Here, it is worth pointing out that the pump–probe signals shown in Fig. 2(a) arise from pump injected exci-

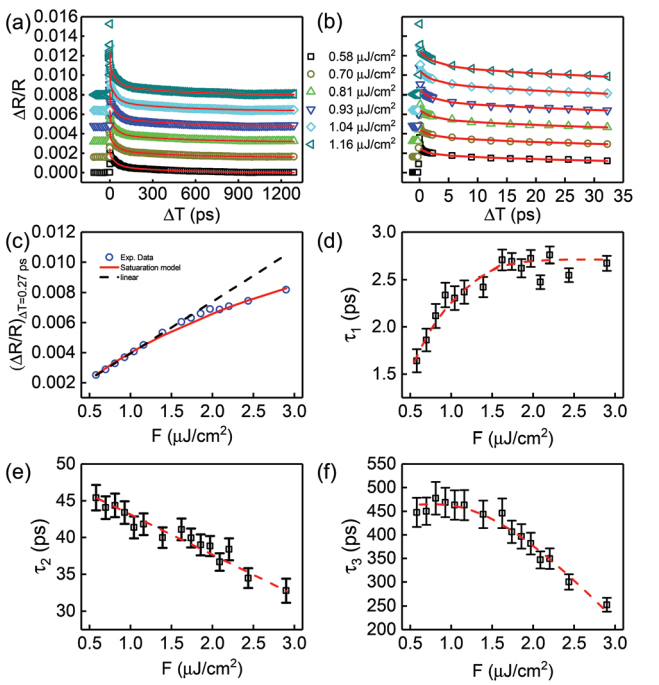

Fig. 2 (a) Transient reflectivity traces under 800 nm degenerate pump–probe measurements at different excitation intensities from 0.58 μJ cm^{-2} to 1.16 μJ cm^{-2}. (b) The zoom in of the first 30 ps of the data shown in (a). (c) Transient reflectivity amplitude at ΔT = 0.27 ps under different pump excitation intensities. The saturation trend above 2.20 μJ cm^{-2} is obvious. The relaxation times τ_1, τ_2, and τ_3 as a function of excitation intensity are shown in (d), (e) and (f), respectively. The red solid lines in (a), (b) and (c) are fitting lines and the red dashed lines in (d), (e) and (f) are eye guiding lines.

Published on 06 November 2017. Downloaded by NANJING UNIVERSITY on 03/12/2017 14:30:00.

tons rather than the line-broadening and peak-shifts which may also be the origin of the pump-induced signals.[25,26] This is confirmed by the consistency of the PL profile and the peak amplitudes of transient reflectivity at different probe energies (Fig. 1(d)). Such an assignment can also be found in other studies.[17,18] These dynamic curves are well described by tri-exponential decay function, indicating that three distinct exciton relaxation channels characterized by τ_1, τ_2 and τ_3 are discovered. Note that one should be aware of that each different time constant does not necessarily mean a different relaxation pathway. As reported by Cooney *et al.*,[27,28] in the QD system, 2–3 different channels contribute to the rate process of electron or hole cooling. Here, our result reveals one more relaxation stage than that reported by Kumar *et al.*[18,23] who only observed two relaxation channels in monolayer $MoSe_2$. A possible reason for this distinction may be that the intra-valley relaxation can be minimized through our degenerate pump probe configuration and thus more refined relaxation dynamics can be observed. More specifically, in the case of the non-degenerate pump probe configuration, the pump-generated excitons are not observed until their transition energy can be accessed by the probe wavelength. In addition to the detailed relaxation processes, the resonant A-exciton transition also allows a very fast exciton generation *via* a photoemission process[2,18,29] as shown in Fig. 2(b) where the rise-up time is as short as 0.27 ps or less.

Fig. 2(c) shows the transient reflectivity amplitude at ΔT = 0.27 ps under different pump excitation intensities. The values of $\Delta R/R$ at ΔT = 0.27 ps increase by a factor of four in the measured pump fluence range, saturating at the highest fluence, which is likely due to the state filling effect near the band edge.[30] To quantify the pump injected excitons, we employ a saturable absorption model[31] to fit to these peak values and obtain the saturation pump fluence density of 3.5 μJ cm^{-2}. The red solid line in Fig. 2(c) represents the fitting line. Using the absorption coefficient of $MoSe_2$ reported in previous work[32] and the measured pump fluence, we estimate the saturant excitation exciton density to be 1.96×10^{11} cm^{-2} which is comparable to the reported values of monolayer $MoSe_2$ in other studies.[23,33] The nonlinear behavior of the peak values of $\Delta R/R$ above 1.74 μJ cm^{-2} also suggests that the photon generated exciton density is close to the highest capacity density. To obtain accurate photon generated exciton density, we calibrated the conversion process of pump power to the pump fluence by measuring the beam spot size carefully (see the ESI†). This process helps to optimize the quantitative analysis discussed later. The τ_1 shown in Fig. 2(d) is found to be increased by two times. A similar fluence dependent relaxation component of the free carrier is also reported by Nie *et al.*[21] in few-layer MoS_2, which is assigned to the hot phonon effect. But in the case of excitons rather than the free carriers, as reported by Robert *et al.*,[34] the thermalization time is about a few tens of ps. Thus, we could exclude the hot phonon effect here. The contribution of the intrinsic radiative exciton lifetime to this short time scale should be ruled out as in the low fluence range it is expected to be independent of the excitation fluence.[35] A possible mechanism accounting for the prolonged fast exciton decay part under a high pump fluence is the surface defect scattering. At low pump fluences photo-excited carriers can quickly relax into the defect states, while with the pump fluence being high, these defect states are filled gradually, leading to the increase of τ_1 and its stabilization eventually. As can be seen in Fig. 2(d), the τ_1 remains constant above 1.62 μJ cm^{-2}. We also noted that some other groups[30] reported a similar pump fluence dependence of exciton relaxation within the timescale of a few ps, claiming that the defect trapping process dominates this behavior. To visualize this exciton relaxation mechanism, we draw the cartoon picture of this process shown in Fig. 4(a) where the defect density is introduced. After the initial fast relaxation into the surface defect states, the populations of excitons are further decreased *via* exciton–exciton annihilation (EEA) as shown in Fig. 2(e) where the relaxation time decreases with increasing the pump fluences. To verify this assignment, we fit a subrange of the transient traces to an exciton–exciton annihilation model that is expressed as follows:[17]

$$N(t) = \frac{N_0}{1 + \gamma N_0 t} \quad (1)$$

where N_0 is the initial photo-generated exciton density and γ is the exciton–exciton annihilation rate. We carefully selected the time zone between ΔT = 5.6 ps and ΔT = 169 ps as the relaxation process of τ_2 and fit the data to eqn (1). According to the fitting results obtained under various pump fluences, we found that the fitted parameter γ above 1.62 μJ cm^{-2} remained almost unchanged indicating that the exciton–exciton annihilation dominated the exciton relaxation in this high pump fluence range. However, for excitation fluences below 1.62 μJ cm^{-2}, the fitted γ values increase with the decrease of excitation intensity (see in Fig. S2†), which suggests that a higher annihilation rate would be required to reduce the population of excitons in the low pump fluence regime. While as reported before by other groups,[17,18] the annihilation rate between excitons in the specific material is constant. Thus, we infer that, in addition to the exciton–exciton annihilation mechanism, one more factor should contribute to the τ_2 decay channel in the low pump excitation range. Meanwhile, it is clearly observed that the pump excitation threshold (1.62 μJ cm^{-2}) below which the γ begins to increase is the same as that where τ_1 begins to decrease (as shown in Fig. 2(d)). Inspired by the similar dependence of τ_1 and γ on the pump fluence, we correlate the defect trapping process of τ_1 with the τ_2 relaxation channel. A generalized rate equation describing the exciton dynamics, where both the EEA process and radiative exciton lifetimes are considered, has been reported.[17,36] In addition, Yu *et al.*[37] also employed the basic EEA differential equation with an additional incident power density term to describe the effect of EEA on luminescence in monolayer TMDs. To better understand the pump fluence dependent coupling strength between the defect trapping and EEA

 This journal is © The Royal Society of Chemistry 2017

Published on 06 November 2017. Downloaded by NANJING UNIVERSITY on 03/12/2017 14:30:00.

process, we introduce constraints into the standard EEA rate equation, written as:

$$\frac{dN}{dt} = -\gamma(N - N_d^{eff})^2$$
$$N(0) = N_0 + N_d^{eff};\ N(\infty) = N_d^{eff} \quad (2)$$

Here, N_0 denotes the initial optical injected exciton population and N_d^{eff} denotes the amount of the excitons trapped by defects at the beginning of EEA (note that N_d^{eff} is a negative value). Since the trapped excitons do not contribute to the exciton–exciton annihilation process, the term N_d^{eff} should be subtracted from the total exciton density N as expressed in eqn (2). The value of N_d^{eff} is fluence dependent rather than time dependent. The solution of the above equation is

$$N(t) = \frac{N_0}{1 + \gamma N_0 t} + N_d^{eff} \quad (3)$$

We also noted that several other papers[38] have reported coupled dynamics between the trap saturation and EEA. Compared to the coupled differential equations proposed in these studies, the modified EEA model in our work (eqn (3)) is very easy to handle, although the former is a more generalized one. The analysis method applied previously in semiconductor quantum dots is also instructive to unravel the details of relaxation pathways and the difference between the relaxation processes.[39,40]

As shown by the red solid fitting lines in Fig. 3(a), we fitted the experimental data very well at low pump fluences using eqn (3) and obtained a shared global fitting parameter γ which is independent of the excitation intensity as τ_2 expected above. The fitted result of γ is 0.4 ± 0.01 $cm^2\ s^{-1}$, which is not only consistent with the value reported by Kumar *et al.*[18] but also the same as that above 1.62 $cm^2\ s^{-1}$ obtained by eqn (1), as shown in Fig. S2.† The fitting result of N_d^{eff} also supports our assignment. In Fig. 3(b), the amplitude N_d^{eff} decreases as the pump fluence increases close to 1.62 μJ cm^{-2} and approximately equals to zero above 1.62 μJ cm^{-2}. The negative sign means the absorbed excitons by defects. As reported by Wang *et al.*,[41] under high exciton density, the exciton–exciton interaction is preferable or more efficient than other mechanisms such as electron–hole recombination and defect scattering. As a result, with the increase of the photo-generated exciton density, the contribution of exciton–exciton annihilation becomes dominant making the defect trapping contribution gradually decrease. More specifically, as the exciton density increases, the effective defect states are gradually fulfilled resulting in the decrease of the amplitude of N_d^{eff}. This finding also suggests that if one wants to avoid the impact of defects on exciton–exciton annihilation, an appropriate selection of pump fluence would work. Similar experimental results have been reported previously in the QD system. Tyagi *et al.*[42,43] have found that, due to surface trapping, high pump fluence can affect exciton dynamics and the exciton annihilation can be controlled *via* surface treatment. These results also uncovered the correlation between defect trapping and EEA.

After being trapped by the defect states that followed by the bi-exciton interaction relaxation, the excitons of monolayer $MoSe_2$ finally relax to an equilibrium state within a long-time scale of a few hundreds of picoseconds, which is usually assigned to both the electron–hole recombination processes.[18,44] At the same time, after τ_1 and τ_2 relaxation processes, the remaining exciton population is far below the threshold where exciton–exciton interaction begins to be dominated. Therefore, many body interactions of excitons can be ignored and we contribute the τ_3 relaxation regime to an isolated exciton recombination process. As shown in Fig. 4(c), both the radiative and non-radiative recombination processes may contribute to the exciton recombination. The wavy line denotes photon emission during the radiative electron–hole recombination. The time scale of the electron–hole recombination in our measurement is consistent with that reported by other groups.[12,45]

However, as shown in Fig. 2(f), the τ_3 values are influenced by pump fluence at a relatively high intensity range, which contradicts the independence of the electron hole recombination lifetime with the pump excitation intensity as reported by Cui *et al.*[35] Considering this, we infer that the τ_3 values are also affected by other factors in the high fluence range. Back

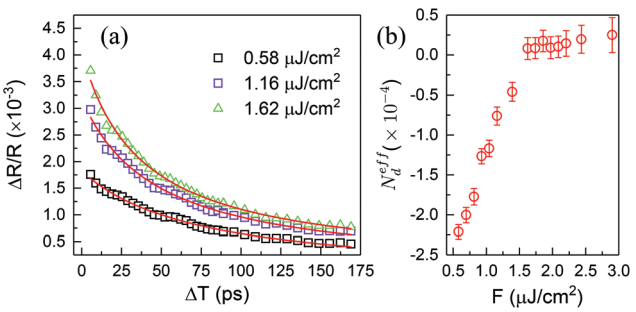

Fig. 3 (a) Transient reflectivity traces at different pump fluences between ΔT = 59 ps and 169 ps. The fitting lines are obtained by the modified exciton–exciton annihilation model (eqn (2)). (b) The coupling term N_d^{eff} increases within the fluence range between 0.58 μJ cm^{-2} and 2.9 μJ cm^{-2}. The values above 1.62 μJ cm^{-2} approximately equal to zero.

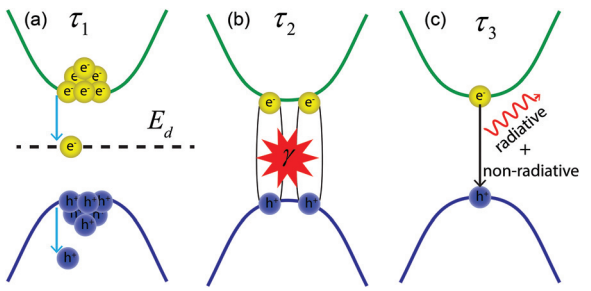

Fig. 4 (a) Excitons are trapped by the defect states. E_d here means the defect energy states. (b) Mutual interactions between excitons that are referred to as the exciton–exciton annihilation and γ is the annihilation rate. (c) Both the radiative and non-radiative electron hole recombinations contribute to the τ_3 relaxation stage. The wavy line denotes photon emission during the radiative process.

Published on 06 November 2017. Downloaded by NANJING UNIVERSITY on 03/12/2017 14:30:00.

to the original experimental data as shown in Fig. S3,† it is clearly observed that the transient $\Delta R/R$ traces are almost overlapped between ΔT = 200 and 400 ps. This period can be safely assigned to the time window of the τ_3 relaxation process as the τ_1 and τ_2 relaxation processes correspond to the time zone before ΔT = 175 ps as shown in Fig. 3(a). Since the transient $\Delta R/R$ traces are overlapped at the beginning of the τ_3 relaxation process, the τ_3 relaxation time should be constant for all the fluences as expected. Whereas after around ΔT = 400 ps, the traces that correspond to the fluences above 1.62 μJ cm^{-2} begin to separate. The up-going trend after ΔT = 400 ps under high pump fluences indicates an additional factor making it difficult for the excitons to relax. Generally, heat diffusion is possible in such a time scale. We also note that the high repetition rate of the pulse laser system would have the possibility to lead to a significant heat accumulation effect if the thermal dissipation in the sample is not efficient enough as discussed by Shi *et al.*[20] Thus, a possible explanation accounting for the behavior of τ_3 under a high pump fluence is the effect of accumulated heat from the pulse laser. Our results indicate that any possible different diffusion rates for different substrates may have different impacts on the behavior of τ_3.

4 Conclusions

In conclusion, we have studied three distinct relaxation channels in monolayer $MoSe_2$ by varying the pump intensity using degenerate ultrafast pump–probe spectroscopy. Our results reveal for the first time the correlation between the different exciton relaxation channels in $MoSe_2$. The exciton–exciton annihilation process is found to be meditated by the defect trapping process that accounts for the initial fast exciton decay at a low pump fluence. We have employed an improved exciton–exciton annihilation model with the introduction of a pump-fluence dependent coupling term and it agrees well with the experimental observation. The final electron–hole recombination is demonstrated to be independent on pump-injected excitons, although it is affected by the heat accumulation under a high excitation intensity. Our findings provide new insights into the exciton relaxation dynamics in terms of the coupled relationship between different decay channels, and at the same time, demonstrate that the pump fluence can be utilized to tune the specific relaxation process, which is important to the potential optoelectronic applications of the TMDC materials.

Author contributions

X. Z. R., F. W., and Y. B. X. conceived the project and Y. B. X supervised the project. Y. Z. M. and F. Q. S. prepared the monolayer $MoSe_2$ samples by the CVD method. B. L. performed ultrafast pump–probe experiments. B. L., X. Z. R., F. W., F. Q. S., W. Q. L., X. F. W., J. W., L. H., R. Z. and Y. B. X. contributed to the analysis of the experiment data. B. L wrote the paper with all authors contributing to the discussion and preparation of the manuscript.

Conflicts of interest

There are no conflicts to declare.

Acknowledgements

This work is supported by the National Basic Research Program of China (2014CB921101); the National Key Research and Development Program of China (2017YFA0206304, 2016YFA0300803); the National Natural Science Foundation of China (61427812, 11774160, 11574137, 61474061, 61674079); Jiangsu Shuangchuang Programme and the Natural Science Foundation of Jiangsu Province of China (BK20140054).

References

1 A. Splendiani, L. Sun, Y. Zhang, T. Li, J. Kim, C.-Y. Chim, G. Galli and F. Wang, *Nano Lett.*, 2010, **10**, 1271–1275.
2 P. Tonndorf, R. Schmidt, P. Böttger, X. Zhang, J. Börner, A. Liebig, M. Albrecht, C. Kloc, O. Gordan, D. R. T. Zahn, S. Michaelis de Vasconcellos and R. Bratschitsch, *Opt. Express*, 2013, **21**, 4908–4916.
3 Z. Yin, H. Li, H. Li, L. Jiang, Y. Shi, Y. Sun, G. Lu, Q. Zhang, X. Chen and H. Zhang, *ACS Nano*, 2012, **6**, 74–80.
4 A. Polman and H. A. Atwater, *Nat. Mater.*, 2012, **11**, 174–177.
5 K. He, N. Kumar, L. Zhao, Z. Wang, K. F. Mak, H. Zhao and J. Shan, *Phys. Rev. Lett.*, 2014, **113**, 026803.
6 M. M. Ugeda, A. J. Bradley, S.-F. Shi, F. H. da Jornada, Y. Zhang, D. Y. Qiu, W. Ruan, S.-K. Mo, Z. Hussain, Z.-X. Shen, F. Wang, S. G. Louie and M. F. Crommie, *Nat. Mater.*, 2014, **13**, 1091–1095.
7 A. Chernikov, T. C. Berkelbach, H. M. Hill, A. Rigosi, Y. Li, O. B. Aslan, D. R. Reichman, M. S. Hybertsen and T. F. Heinz, *Phys. Rev. Lett.*, 2014, **113**, 076802.
8 G. Wang, X. Marie, I. Gerber, T. Amand, D. Lagarde, L. Bouet, M. Vidal, A. Balocchi and B. Urbaszek, *Phys. Rev. Lett.*, 2015, **114**, 097403.
9 F. Withers, O. Del Pozo-Zamudio, S. Schwarz, S. Dufferwiel, P. M. Walker, T. Godde, A. P. Rooney, A. Gholinia, C. R. Woods, P. Blake, S. J. Haigh, K. Watanabe, T. Taniguchi, I. L. Aleiner, A. K. Geim, V. I. Fal'ko, A. I. Tartakovskii and K. S. Novoselov, *Nano Lett.*, 2015, **15**, 8223–8228.
10 F. Withers, O. Del Pozo-Zamudio, A. Mishchenko, A. P. Rooney, A. Gholinia, K. Watanabe, T. Taniguchi, S. J. Haigh, A. K. Geim, A. I. Tartakovskii and K. S. Novoselov, *Nat. Mater.*, 2015, **14**, 301–306.
11 A. Pospischil, M. M. Furchi and T. Mueller, *Nat. Nanotechnol.*, 2014, **9**, 257–261.

 This journal is © The Royal Society of Chemistry 2017

Published on 06 November 2017. Downloaded by NANJING UNIVERSITY on 03/12/2017 14:30:00.

12 T. Korn, S. Heydrich, M. Hirmer, J. Schmutzler and C. Schuller, *Appl. Phys. Lett.*, 2011, **99**, 102109.
13 G. Wang, L. Bouet, D. Lagarde, M. Vidal, A. Balocchi, T. Amand, X. Marie and B. Urbaszek, *Phys. Rev. B: Condens. Matter*, 2014, **90**, 075413.
14 G. Wang, E. Palleau, T. Amand, S. Tongay, X. Marie and B. Urbaszek, *Appl. Phys. Lett.*, 2015, **106**, 112101–112105.
15 M. Palummo, M. Bernardi and J. C. Grossman, *Nano Lett.*, 2015, **15**, 2794–2800.
16 H. Wang, C. Zhang, W. Chan, C. Manolatou, S. Tiwari and F. Rana, *Phys. Rev. B: Condens. Matter*, 2016, **93**, 045407.
17 D. Sun, Y. Rao, G. A. Reider, G. Chen, Y. You, L. Brézin, A. R. Harutyunyan and T. F. Heinz, *Nano Lett.*, 2014, **14**, 5625–5629.
18 N. Kumar, Q. N. Cui, F. Ceballos, D. W. He, Y. S. Wang and H. Zhao, *Phys. Rev. B: Condens. Matter*, 2014, **89**, 125427.
19 H. Wang, C. Zhang and F. Rana, *Nano Lett.*, 2015, **15**, 339–345.
20 H. Shi, R. Yan, S. Bertolazzi, J. Brivio, B. Gao, A. Kis, D. Jena, H. G. Xing and L. Huang, *ACS Nano*, 2013, **7**, 1072–1080.
21 Z. Nie, R. Long, L. Sun, C.-C. Huang, J. Zhang, Q. Xiong, D. W. Hewak, Z. Shen, O. V. Prezhdo and Z.-H. Loh, *ACS Nano*, 2014, **8**, 10931–10940.
22 J. C. Shaw, H. Zhou, Y. Chen, N. O. Weiss, Y. Liu, Y. Huang and X. Duan, *Nano Res.*, 2014, **7**, 511–517.
23 N. Kumar, Q. Cui, F. Ceballos, D. He, Y. Wang and H. Zhao, *Nanoscale*, 2014, **6**, 4915–4919.
24 X. Wang, Y. Gong, G. Shi, W. L. Chow, K. Keyshar, G. Ye, R. Vajtai, J. Lou, Z. Liu, E. Ringe, B. K. Tay and P. M. Ajayan, *ACS Nano*, 2014, **8**, 5125–5131.
25 S. Sim, J. Park, J.-G. Song, C. In, Y.-S. Lee, H. Kim and H. Choi, *Phys. Rev. B: Condens. Matter*, 2013, **88**, 075434.
26 C. Ruppert, A. Chernikov, H. M. Hill, A. F. Rigosi and T. F. Heinz, *Nano Lett.*, 2017, **17**, 644–651.
27 R. R. Cooney, S. L. Sewall, K. E. H. Anderson, E. A. Dias and P. Kambhampati, *Phys. Rev. Lett.*, 2007, **98**, 177403.
28 R. R. Cooney, S. L. Sewall, E. A. Dias, D. M. Sagar, K. E. H. Anderson and P. Kambhampati, *Phys. Rev. B: Condens. Matter*, 2007, **75**, 245311.
29 S. Tongay, J. Zhou, C. Ataca, K. Lo, T. S. Matthews, J. Li, J. C. Grossman and J. Wu, *Nano Lett.*, 2012, **12**, 5576–5580.
30 M. Seo, H. Yamaguchi, A. D. Mohite, S. Boubanga-Tombet, J.-C. Blancon, S. Najmaei, P. M. Ajayan, J. Lou, A. J. Taylor and R. P. Prasankumar, *Sci. Rep.*, 2016, **6**, 21601.
31 R. W. Boyd, *Nonlinear Optics*, Academic Press, 2003.
32 A. R. Beal and H. P. Hughes, *J. Phys. C: Solid State Phys.*, 1979, **12**, 881–890.
33 N. Kumar, J. He, D. He, Y. Wang and H. Zhao, *Nanoscale*, 2014, **6**, 12690–12695.
34 C. Robert, D. Lagarde, F. Cadiz, G. Wang, B. Lassagne, T. Amand, A. Balocchi, P. Renucci, S. Tongay, B. Urbaszek and X. Marie, *Phys. Rev. B: Condens. Matter*, 2016, **93**, 205423.
35 Q. Cui, F. Ceballos, N. Kumar and H. Zhao, *ACS Nano*, 2014, **8**, 2970–2976.
36 L. Yuan and L. Huang, *Nanoscale*, 2015, **7**, 7402–7408.
37 Y. Yu, Y. Yu, C. Xu, A. Barrette, K. Gundogdu and L. Cao, *Phys. Rev. B: Condens. Matter*, 2016, **93**, 201111.
38 T. S. Sosnowski, T. B. Norris, H. H. Wang, P. Grenier, J. F. Whitaker and C. Y. Sung, *Appl. Phys. Lett.*, 1997, **70**, 3245–3247.
39 P. Kambhampati, *Acc. Chem. Res.*, 2011, **44**, 1–13.
40 S. Banerjee, S. Maity and A. Datta, *J. Phys. Chem. C*, 2011, **115**, 22804–22809.
41 H. Wang, J. H. Strait, C. Zhang, W. Chan, C. Manolatou, S. Tiwari and F. Rana, *Phys. Rev. B: Condens. Matter*, 2015, **91**, 165411.
42 P. Tyagi, R. R. Cooney, S. L. Sewall, D. M. Sagar, J. I. Saari and P. Kambhampati, *Nano Lett.*, 2010, **10**, 3062–3067.
43 P. Tyagi and P. Kambhampati, *J. Chem. Phys.*, 2011, **134**, 094706–094711.
44 Q. Wang, S. Ge, X. Li, J. Qiu, Y. Ji, J. Feng and D. Sun, *ACS Nano*, 2013, **7**, 11087–11093.
45 D. Lagarde, L. Bouet, X. Marie, C. R. Zhu, B. L. Liu, T. Amand, P. H. Tan and B. Urbaszek, *Phys. Rev. Lett.*, 2014, **112**, 047401.